Supporting Information

Cregg et al. 10.1073/pnas.1711536114

SI Materials and Methods

Animals. All animal procedures were approved by the Case Western Reserve University IACUC. The following mice were obtained from The Jackson Laboratory: *Vglut2*^{Cre} (stock #016963), *Phox2b*^{Cre} (#016223), *Atoh1*^{Cre} (#011104), *Vgat*^{Cre} (#016962), *R26R*$^{ChR2\text{-}EYFP}$ (#012569), *R26R*^{LacZ} (#012429), and *Tau*$^{lsl\text{-}LacZ}$ (#021162). Mice were maintained on a mixed background. *Vglut2*^{Cre}, *Phox2b*^{Cre}, *Atoh1*^{Cre}, or *Vgat*^{Cre} mice were crossed to *R26R*$^{ChR2\text{-}EYFP}$, *R26R*^{LacZ}, or *Tau*$^{lsl\text{-}LacZ}$ reporter mice, and heterozygous alleles were used for experiments. Animals were assigned to groups based on genotype, and experiments were performed with prior knowledge of genotype. Wild-type C57BL/6J mice (stock #000664) were used in experiments which did not require genetic perturbations. We used P2–P4 male/female mice for all experiments herein.

Dissection. Mice were anesthetized, decapitated at the level of the midbrain, and eviscerated. Rapid dissection was carried out in room temperature oxygenated Ringer's solution (23–26 °C, 95% O_2/5% CO_2, pH 7.4), composed of 128 mM NaCl, 4 mM KCl, 21 mM $NaHCO_3$, 0.5 mM NaH_2PO_4, 2 mM $CaCl_2$, 1 mM $MgCl_2$, and 30 mM D-glucose. The central nervous system was exposed ventrally, and phrenic nerves were dissected free from connective tissue. In a subset of experiments, fictive inspiration was initiated by transection at the pontomedullary boundary just rostral to the anterior inferior cerebellar artery (Fig. S1 *E* and *F*). Additionally, in experiments utilizing PTX/STRYCH, we sectioned caudally at C8 (8).

Electrophysiology and Photostimulation. Recording was carried out under continuous perfusion of control aCSF (same composition as above) or 80% O_2/20% CO_2-equilibrated aCSF to simulate respiratory acidosis. Suction electrodes were attached to the phrenic nerve, hypoglossal nerve, and/or the L1 ventral root. Signal was filtered from 30 Hz to 1 kHz using Grass amplifiers, amplified 10,000×, and sampled using a Digidata 1440A (Molecular Devices) at a rate of 50 kHz. A Polychrome V halogen lamp was used for photostimulation, and blue light was directed at the hindbrain using a fiberoptic light guide (wavelength, 473 nm; 15-nm bandwidth; Till Photonics). The spatial extent of light illumination for each experiment is represented in accompanying illustrations. Light intensity was measured with a photodiode (catalog #S120C; Thorlabs) coupled to a power meter (catalog #PM100D; Thorlabs). The light intensity used herein was ∼0.20 $mW{\cdot}mm^{-2}$. This low level of continuous blue light maintained responses throughout the duration of the photostimulus (Figs. 1–4; see also ref. 8), indicating that continuous photostimulation did not cause conduction block or tissue damage. We did not observe any electrophysiological response to photostimulation in monoallelic Cre- or *R26R*$^{ChR2\text{-}EYFP}$ strains, which indicates that Cre-mediated recombination of the *Rosa26* locus is required for ChR2-EYFP expression and that photostimulation does not cause ChR2-independent effects. We used the following drugs: picrotoxin (PTX) ($GABA_A$R antagonist, 10 μM; Sigma), strychnine hydrochloride (STRYCH) (GlyR antagonist, 0.3 μM; Sigma), prazosin hydrochloride (PRAZ) (α_1-AR antagonist, 25 μM; Sigma), propranolol (PROP) (β-AR antagonist, 25 μM; Sigma), and substance P acetate salt hydrate (substance P) (neurokinin 1 receptor agonist, 1 μM; Sigma).

Analysis. Data were recorded using AxoScope software (Molecular Devices) and analyzed in Spike2 (Cambridge Electronic Design). Signal was processed to remove DC drift, and integrated traces are presented as rectified and smoothed (0.1–0.2 s) electroneurographs. For individual traces, we quantified burst event time and duration with respect to light onset. Raster plots were constructed in R (R Project). Individual trials were aligned by light onset, and individual bursts are represented by black rectangles. Gray boxes group together technical replicates from a single biological replicate. Instantaneous frequency (f) was calculated continuously every 0.1 s over 24 trials (bin = 5 s). Half-life ($t_{1/2}$) of rebound effects were estimated by exponential regression fitting of f. Rebound bursts were defined as those occurring within 3 s of an inhibitory stimulus. Based on data from pontomedullary preparations (Fig. 1 *A* and *B*), we estimate the false-positive rate to be <0.2% for aCSF, and 30–35% after application of PTX/STRYCH. Phase relationships between PN and L1 were determined using circular plot analysis (52), where each point represents the average vector magnitude/direction for a single biological replicate and the arrow represents the group-averaged magnitude/direction (0 is synchronous and π is asynchronous, 1 cycle = 2π rad = 360°).

Statistics. Statistical analysis was performed in JMP, version 11 (SAS). Power analysis was used to determine minimum sample size. We used Shapiro–Wilk to test for normality. For data which did not exhibit a normal distribution, we used a Mann–Whitney U test followed by Bonferroni correction for multiple comparisons. For data exhibiting a normal distribution, we used Brown–Forsythe to test for equivalent variance. For cases of equivalent variance, a t test was used for single comparisons, and a one-way ANOVA followed by Tukey–Kramer honest significant difference (HSD) post hoc was used for multiple comparisons. A Welch ANOVA was used in cases of unequal variance, followed by Bonferroni correction for multiple comparisons. $P < 0.05$ was considered to be statistically significant, where $^*P < 0.05$, $^{**}P < 0.01$, and $^{***}P < 0.001$. Data are presented as mean ± SEM; $n = 8$ biological replicates for each group, unless stated otherwise. In box-and-whisker plots, whiskers represent the range excluding outliers.

X-Gal Staining and Imaging. Postdissection, tissue was fixed for 30 min in 4% paraformaldehyde and subsequently washed in PBS. On a subset of samples ($n = 8$ per genotype), we performed whole-mount X-gal staining for 2 h at 37 °C, which allowed X-gal substrate to react with LacZ-expressing cells positioned within 152 ± 13 μm ($n = 3$) of the tissue surface. The remaining samples ($n = 8$ per genotype) were sectioned at 20 μm with a cryostat, and X-gal stained overnight at 37 °C. We captured bright-field whole-mount images using a stereomicroscope (Zeiss). Sections were imaged using a Leitz Orthoplan 2 upright bright-field microscope.

High-Speed Video. A Retiga EXi camera (QImaging) attached to a Navitar Zoom 7000 lens was used to capture high-speed video of ribcage movements [10–50 frames per second (f.p.s.)]. Images were acquired using QCapture Pro-6 (QImaging) and Micromanager 1.4 (Micromanager) software. Ribcage movements were quantified in ImageJ, using the outermost point of a single rib for x–y measurements.

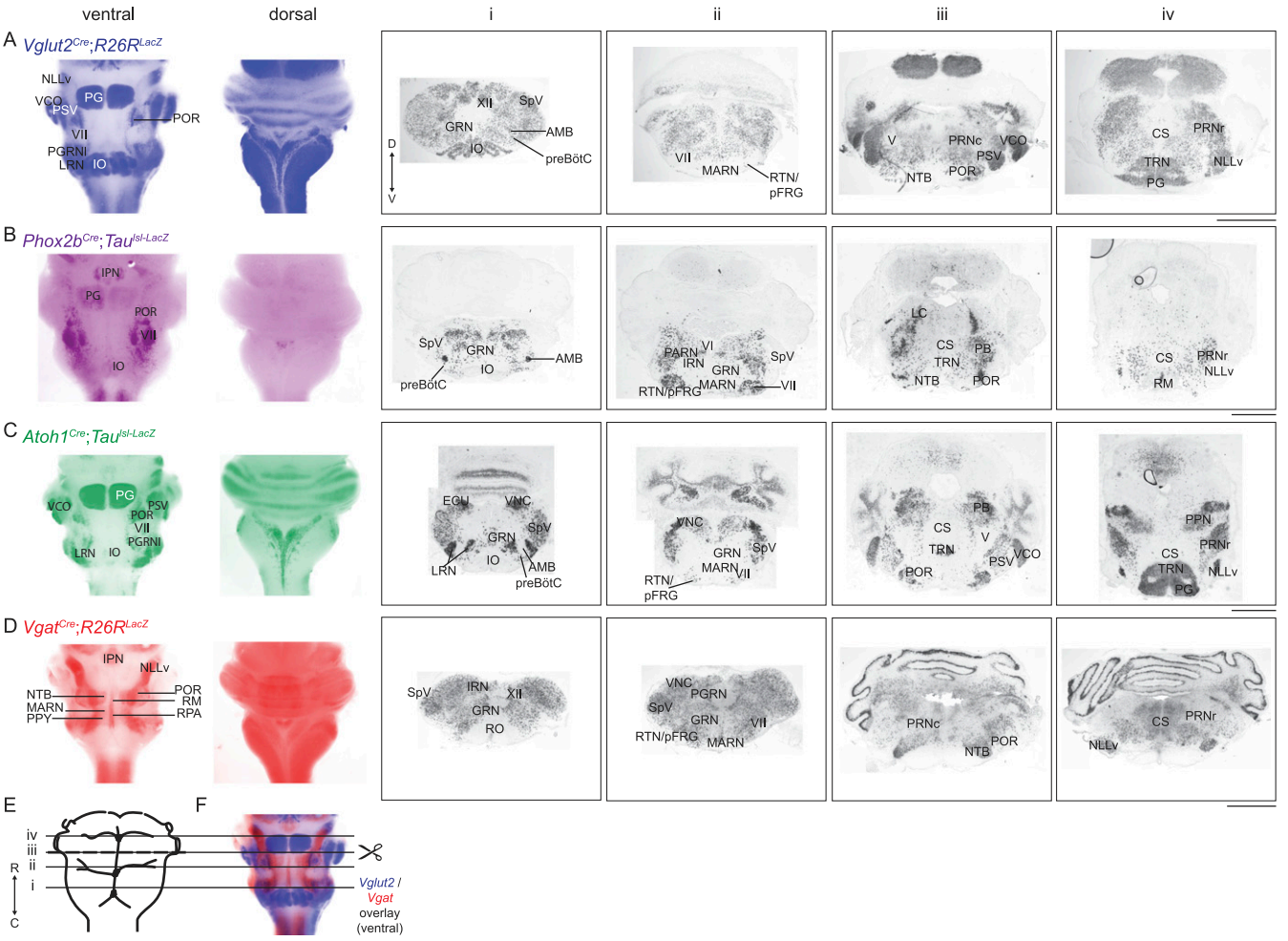

Fig. S1. Characterization of Cre-recombinase alleles. (*A*) X-gal staining for LacZ expression in *Vglut2*^{Cre};*R26R*^{LacZ} mice. (*Left*) Whole-mount staining. Hindbrain pseudocolored blue. (*Right*) Selected sections from four coronal planes (see schematic at *Bottom*). (*B–D*) X-gal staining for LacZ expression in *Phox2b*^{Cre};*Tau*$^{lsl\text{-}LacZ}$, *Atoh1*^{Cre};*Tau*$^{lsl\text{-}LacZ}$, and *Vgat*^{Cre};*R26R*^{LacZ} mice, respectively. Whole-mount images are pseudocolored purple, green, and red, respectively. LacZ expression closely matches Cre-recombinase expression patterns characterized for these alleles previously (49–51). (*E*) Illustration of the hindbrain in relationship to brainstem vasculature, and the approximate level of transverse coronal sections in *A–D*. For experiments initiating fictive inspiration, the pons was removed by transection at level iii. (*F*) A whole-mount overlay demonstrates that brainstem nuclei enriched for Vglut2+ neurons are generally less enriched for Vgat+ neurons and vice versa, indicating that these genes mark terminally differentiated, nonoverlapping populations of excitatory and inhibitory neurons, respectively (49). (Scale bars, 1 mm.) Arrows indicate rostral (R), caudal (C), dorsal (D), and ventral (V) directions. Abbreviations: AMB, nucleus ambiguus; CS, superior central nucleus raphé; ECU, external cuneate nucleus; GRN, gigantocellular reticular nucleus; IO, inferior olivary complex; IPN, interpeduncular nucleus; IRN, intermediate reticular nucleus; LC, locus coeruleus; LRN, lateral reticular nucleus; MARN, magnocellular reticular nucleus; NLLv, nucleus of the lateral lemniscus, ventral part; NTB, nucleus of the trapezoid body; PARN, parvicellular reticular nucleus; PB, parabrachial nucleus; PG, pontine gray; PGRNl, paragigantocellular reticular nucleus, lateral; POR, superior olivary complex, periolivary region; PPN, pedunculopontine nucleus; PPY, parapyramidal nucleus; PRNc, pontine reticular nucleus, caudal; preBötC, pre-Bötzinger complex; PRNr, pontine reticular nucleus, rostral; PSV, principal sensory nucleus of the trigeminal; RM, nucleus raphé magnus; RO, nucleus raphé obscurus; RPA, nucleus raphé pallidus; RTN/pFRG, retrotrapezoid nucleus/parafacial respiratory group; SpV, spinal nucleus of the trigeminal; TRN, tegmental reticular nucleus; V, motor nucleus of trigeminal; VCO, ventral cochlear nucleus; VI, abducens nucleus; VII, facial motor nucleus; VNC, vestibular nuclei; XII, hypoglossal motor nucleus.

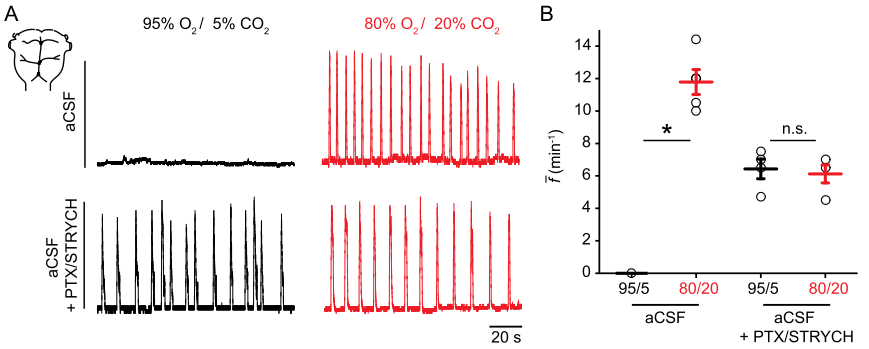

Fig. S2. The inspiratory response to hypercapnia is dependent on inhibitory synaptic transmission. (*A*) Phrenic nerve recordings from pontomedullary preparations. (*Top Left*) No spontaneous inspiratory bursting is observed under normocapnic (95% O_2/5% CO_2) conditions. (*Top Right*) Hypercapnic aCSF (80% O_2/20% CO_2) causes rapid inspiratory bursting. (*Bottom Left*) After application of PTX/STRYCH, pontomedullary preparations exhibit a baseline frequency of 4–7 min^{-1}. (*Bottom Right*) PTX/STRYCH application blocks hypercapnia-induced increases in *f* above baseline. (*B*) Quantification of average *f* in response to hypercapnia. PTX/STRYCH application blocks hypercapnia-induced increases in *f*. *$P = 0.04$. Mann–Whitney *U* test with Bonferroni correction. $n = 5$ for aCSF, $n = 4$ for aCSF + PTX/STRYCH. Data are mean ± SEM.

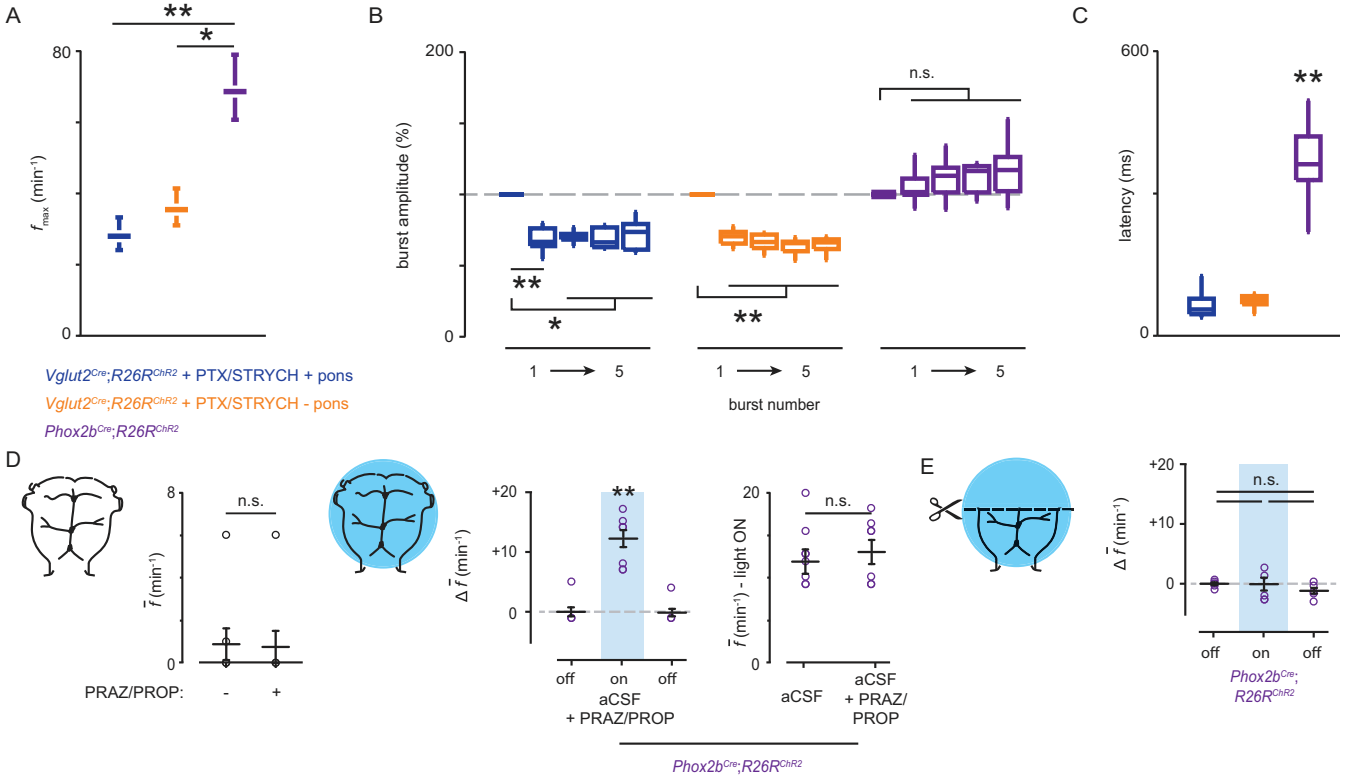

Fig. S3. *Phox2b*^{Cre};*R26R*^{ChR2}-mediated increases in *f* compared with *Vglut2*^{Cre};*R26R*^{ChR2} + PTX/STRYCH-induced excitation. (*A*) f_{max} in response to stimulation of Phox2b+ neurons was much faster than f_{max} during stimulation of Vglut2+ neurons in the absence of inhibition. *Phox2b* vs. *Vglut2* + PTX/STRYCH + pons, **$P = 0.005$. *Phox2b* vs. *Vglut2* + PTX/STRYCH − pons, *$P = 0.04$. Mann–Whitney *U* test with Bonferroni correction. $n = 8$ for each condition; error bars represent SEM. (*B*) Stimulation of Vglut2+ neurons in the presence of PTX/STRYCH resulted in smaller inspiratory burst amplitude for successive bursts. *Vglut2* + PTX/STRYCH + pons, burst #1 vs. #2–5: *$P < 0.05$ and **$P < 0.01$. *Vglut2* + PTX/STRYCH − pons, burst #1 vs. #2–5, **$P = 0.004$. Mann–Whitney *U* test with Bonferroni correction. Stimulation of Phox2b+ neurons (purple) did not result in depression of burst amplitude upon successive bursts (no significance, Mann–Whitney *U* test). $n = 8$ for each condition; whiskers represent range. Bursts are numbered beginning with the first burst observed in response to the photostimulus. (*C*) Whereas the response latency following stimulation of Vglut2+ neurons exhibited minimal delay (~100 ms), stimulation of Phox2b+ neurons evoked an inspiratory burst at a significant delay (367 ± 30 ms). *Phox2b* vs. *Vglut2* + PTX/STRYCH + pons, **$P = 0.003$. *Phox2b* vs. *Vglut2* + PTX/STRYCH − pons, **$P = 0.003$. Mann–Whitney *U* test with Bonferroni correction. $n = 8$ for each condition; whiskers represent range. (*D*) *Phox2b*^{Cre};*R26R*^{ChR2} mediated increases in *f* were insensitive to application of the α_1- and β-adrenergic receptor antagonists propranolol and prazosin (+PRAZ/PROP), which block catecholaminergic neurotransmission. (*Left*) Application of PRAZ/PROP had no effect on baseline *f* in pontomedullary preparations (no significance, Mann–Whitney *U* test). (*Middle*) Baseline vs. photostimulation, **$P = 0.002$. Photostimulation vs. after light, **$P = 0.002$. Mann–Whitney *U* test with Bonferroni correction. (*Right*) No significance, Mann–Whitney *U* test. $n = 8$ for each condition. Data are mean ± SEM. (*E*) *Phox2b*^{Cre};*R26R*^{ChR2}-mediated increases in *f* required an intact pons (no significance, Welch's ANOVA). $n = 6$ mice. Data are mean ± SEM.

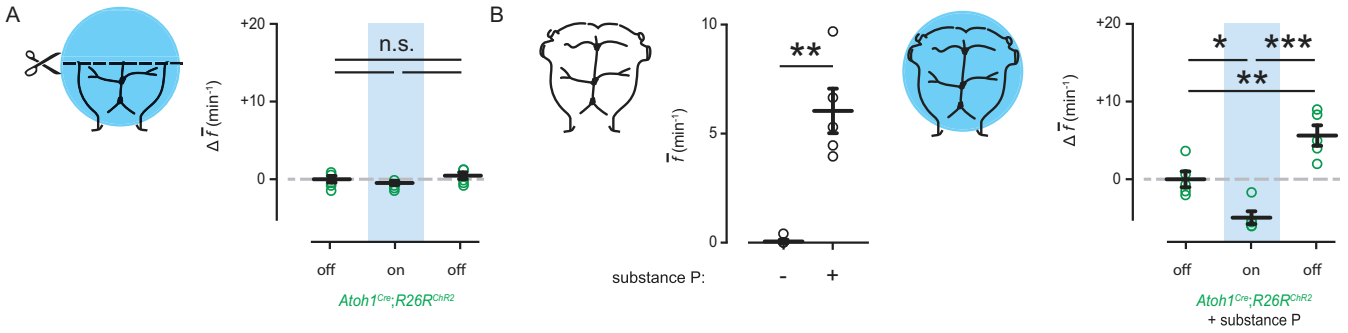

Fig. S4. *Atoh1*^{Cre};*R26R*^{ChR2} suppression of substance P initiated inspiratory bursting. (*A*) *Atoh1*^{Cre};*R26R*^{ChR2} response required an intact pons (compare with Fig. 2 *E* and *H*; no significance, one-way ANOVA). $n = 5$ mice. (*B*) In pontomedullary preparations, stimulation of Atoh1+ neurons suppressed substance P-evoked bursting. *$P = 0.017$ baseline vs. photostimulation, ***$P = 4.1 \times 10^{-5}$ photostimulation vs. after light, **$P = 0.007$ baseline vs. after light, one-way ANOVA and post hoc Tukey–Kramer HSD. $n = 5$ mice. Data are mean ± SEM.

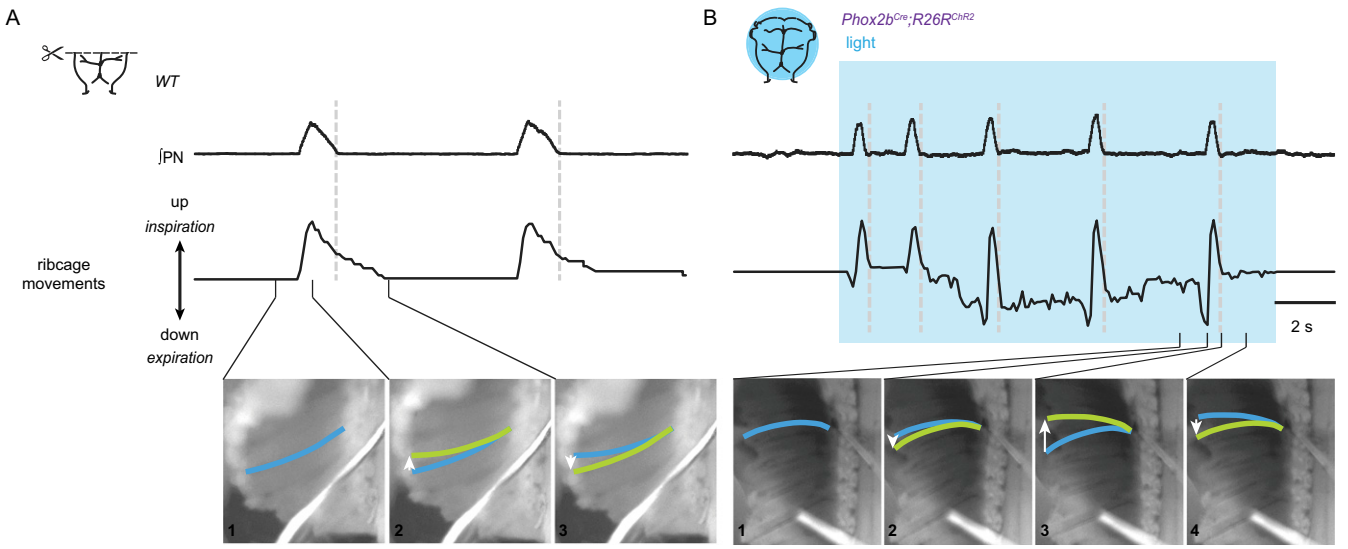

Fig. S5. High-speed video demonstrates two distinct modes of inspiration. (*A*, *Top*) During fictive inspiration, phrenic bursts exhibited a low frequency and long duration. (*Middle*) Simultaneous quantification of ribcage movement indicated no active expiratory (downward) movement during fictive inspiration, and in contrast, the ribcage exhibited passive recoil, returning to its original position long after termination of the inspiratory burst. (*B*, *Top*) Stimulation of Phox2b+ neurons caused high-frequency inspiratory bursts. (*Middle*) Simultaneous quantification of ribcage movement indicated an active expiratory (downward) phase, which was quickly followed by an upward ribcage deflection. The ribcage then returned to its original position upon termination of phrenic inspiratory bursts. The traces of PN and ribcage movements (*Top*) are linked with video frames (*Bottom*) which correspond to the time points indicated in the trace. Blue line indicates the original position of a single rib from previous image, and a green line indicates current (final) position of the rib.

Table S1. Definition of terms

Term	Variable	Units	Definition
Inspiratory frequency	f	min^{-1}	Instantaneous phrenic burst frequency measured relative to light onset and across trials, bin = 5 s
Average inspiratory frequency	$\bar{f}$	min^{-1}	Average phrenic burst frequency over a given time interval
Change in average inspiratory frequency	$\Delta\bar{f}$	min^{-1}	Change in average frequency relative to a prestimulus baseline normalized to 0
Minimum interburst interval	IBI_{min}	s	Time between the first two bursts observed in response to photostimulation
Maximum inspiratory frequency	f_{max}	min^{-1}	Inverse of IBI_{min}
Latency		ms	Time between onset of photostimulation and unit/burst response in raw trace

Table S2. Summary of results

Genotype/treatment	±Pons	$\bar{f}$, min^{-1}	↑ or ↓ relative to baseline	PTX/STRYCH sensitive?	Interpretation
WT	–	4.94 ± 0.30	Baseline	No	Baseline
WT	+	0.08 ± 0.05	↓	Yes	Inhibition
$Vglut2^{Cre};R26R^{ChR2}$	+	14.29 ± 0.76	↑	No	Excitation
$Vglut2^{Cre};R26R^{ChR2}$	–	13.25 ± 0.63	↑	No	Excitation
$Phox2b^{Cre};R26R^{ChR2}$	+	16.13 ± 1.45	↑	Yes	Phasic Inhibition
WT + CO_2	+	11.78 ± 0.77	↑	Yes	Phasic Inhibition
$Atoh1^{Cre};R26R^{ChR2}$ + Substance P	+	1.10 ± 0.82	↓	Yes	Inhibition
$Vgat^{Cre};R26R^{ChR2}$ continuous light	–	0.31 ± 0.15	↓	Yes	Inhibition
$Vgat^{Cre};R26R^{ChR2}$ pulsed light	+	9.54 ± 0.17	↑	Yes	Phasic Inhibition

Inhibition is a decrease in *f* which is PTX/STRYCH sensitive. Disinhibition (i.e., PTX/STRYCH application) only relieves inhibition, returning *f* to baseline; disinhibition cannot increase *f* above baseline. Excitation is an increase in *f* which is insensitive to application of PTX/STRYCH. Phasic inhibition is an increase in *f* which is PTX/STRYCH sensitive. We distinguish phasic inhibition from disinhibition on the basis of the postsynaptic response; whereas disinhibition only relieves inhibition, phasic inhibition causes a rebound inspiratory burst. Data are mean ± SEM.

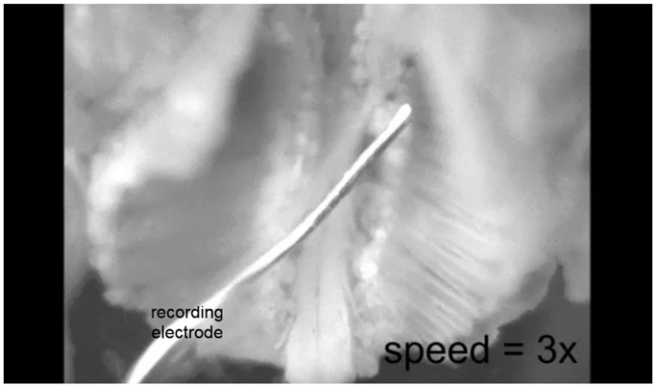

Movie S1. Related to Fig. S5. High-speed video demonstrates two distinct modes of inspiration. First, fictive inspiration initiated by removal of the pons. Upward, but not downward, ribcage movements are visible. Movie is sped up three times. Second, stimulation of Phox2b+ neurons causes downward ribcage movement followed by upward deflection of the ribcage. 1 f.p.s., 1 frame per second. Arrowhead points to one rib. Third, direct comparison of fictive inspiration in preparations lacking the pons with inspiration initiated by stimulation of Phox2b+ neurons. Both fictive inspiration and Phox2b-evoked inspiration are sped up 1.5 times.

Movie S1